AEDC-TDR-64-256

GENERAL CONSIDERATIONS OF MHD ACCELERATION FOR AERODYNAMIC TESTING

By

Leon E. Ring
Propulsion Wind Tunnel Facility
ARO, Inc.

TECHNICAL DOCUMENTARY REPORT NO. AEDC-TDR-64-256

December 1964

Program Element 61405014/8951, 895101

(Prepared under Contract No. AF 40(600)-1000 by ARO, Inc., contract operator of AEDC, Arnold Air Force Station, Tenn.)

ARNOLD ENGINEERING DEVELOPMENT CENTER
AIR FORCE SYSTEMS COMMAND
UNITED STATES AIR FORCE

NOTICES

Qualified requesters may obtain copies of this report from DDC, Cameron Station, Alexandria, Va. Orders will be expedited if placed through the librarian or other staff member designated to request and receive documents from DDC.

When Government drawings, specifications or other data are used for any purpose other than in connection with a definitely related Government procurement operation, the United States Government thereby incurs no responsibility nor any obligation whatsoever; and the fact that the Government may have formulated, furnished, or in any way supplied the said drawings, specifications, or other data, is not to be regarded by implication or otherwise as in any manner licensing the holder or any other person or corporation, or conveying any rights or permission to manufacture, use, or sell any patented invention that may in any way be related thereto.

GENERAL CONSIDERATIONS OF MHD ACCELERATION FOR AERODYNAMIC TESTING

By

Leon E. Ring

Propulsion Wind Tunnel

ARO, Inc.

a subsidiary of Sverdrup and Parcel, Inc.

Presented at the AGARD Specialists' Meeting on "Arc Heaters and MHD Accelerators for Aerodynamic Purposes," 21-23 September 1964, Rhode-Saint-Genese, Belgium.

December 1964

AF - AEDC
Arnold AFS Tenn

ABSTRACT

Estimates of magnetohydrodynamic (MHD) accelerator performance limitations show that velocities of 30,000 to 40,000 ft/sec at high density should be attainable with a Faraday accelerator. Operation near atmospheric pressure using seeded air is suggested; order of magnitude estimates indicate the seed material should not affect most aerodynamic testing. The possibility of increased performance by using nonequilibrium electrical conductivity is discussed.

PUBLICATION REVIEW

This report has been reviewed and publication is approved.

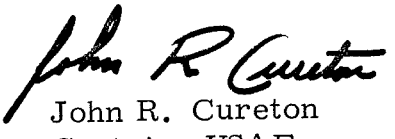

John R. Cureton
Captain, USAF
Gas Dynamics Division
DCS/Research

Donald R. Eastman, Jr.
DCS/Research

CONTENTS

ILLUSTRATIONS

Figure

NOMENCLATURE

A	Channel cross-sectional area
B	Magnetic field of induction
b	Ion slip parameter, Eq. (8)
E	Electric field
e	Electronic charge
H	Total enthalpy, $(u^2/2) + h$
h	Static enthalpy
J	Total current
j	Current density
k	Boltzmann's constant
L	Channel length, also body characteristic length
M	Mach number
m	Particle mass
n	Particle number density
P	Power
p	Pressure
R	Gas constant
S	Entropy
T	Temperature
u	Velocity
V	Voltage
x, y, z	Channel coordinates, Fig. 4b
Z*	Moles per mole of gas at low temperature
α	Ionization fraction
β	uB/Ey
β_H	uB/E_H
Δ	Increment of same quantity
δ	Electron energy loss coefficient; also shock standoff distance
η	Accelerator energy transfer efficiency

θ	Mass fraction of seed material
μ	Magnetic permeability
ρ	Gas density
σ	Electrical conductivity
ϕ	Parameter defined in Eq. (7)
$\omega\tau$	Product of cyclotron frequency times mean collision time for electron collisions with heavy particles
$(\omega\tau)_I$	Product of cyclotron frequency times mean collision time for ion-neutral particle collisions

SUBSCRIPTS

o	Stagnation or reservoir conditions
1	Accelerator inlet
2	Accelerator exit
e	Electrons
g	Gas
H	Hall
n	Neutral
x	x-component
y	y-component

1.0 INTRODUCTION

The limitations of conventional hypervelocity simulation techniques have become apparent in recent years. Continuous facilities, facilities with testing time of seconds to minutes, are limited by electric-arc-heater performance. The performance limit of current electric-arc-heaters was given by Cann and Buhler (Ref. 1 and shows the limit to be about 100 atm pressure at moderate enthalpies. Higher performance can be obtained in short duration facilities such as a reflected shock tunnel, which gives testing time of milliseconds. The performance limit of a reflected shock tunnel was recently discussed by Bird, et al. (Ref. 2), who concluded that reservoir conditions will be limited to about 2000 atm pressure at 9000°K.

A method of extending the simulation capabilities is the use of magnetohydrodynamic (MHD) accelerators. This was suggested by Boison and Ring (Ref. 3) for a large facility and allows direct kinetic energy addition to the flow, alleviating the containment problem of high-pressure, high-temperature gases. In a sense, MHD techniques offer the first promise of a quantum increase in aerodynamic test capabilities since the introduction of shock-tube, shock-tunnel techniques a number of years ago. The impact on testing will no doubt be comparable.

Although a quantum increase in test capability may result, MHD accelerators are not to be viewed as an ultimate and have definite limitations regarding free-stream chemical state and the purity of the test gas. Also, there are definite limits in terms of velocity and density of the flow which can be obtained. In this report, an effort will be made to establish these limitations, and estimates of expected accelerator performance will be made for both continuous and short duration testing. The promising modes of accelerator operation will be indicated in terms of pressure level, temperature level, and velocities.

It should be pointed out that the interest here is in "aerodynamic" testing and not simply "stagnation point heat transfer" testing.

2.0 SIMULATION

2.1 SIMULATION REQUIREMENTS

Conventional techniques are adequate for aerodynamic testing in the perfect gas regime, where Mach number and Reynolds number are the

---

Manuscript received November 1964.

important parameters. Therefore, any consideration of MHD techniques should be limited to where real gas effects are important: dissociation, ionization, and recombination. By considering the oxygen dissociation and recombination reaction rates, Harney (Ref. 4) has shown that in the range of practical flight the flow chemistry is neither frozen nor in equilibrium so the finite rate chemistry must be simulated; that is, in the range from 100,000 to 300,000 ft altitude and above 13,000 ft/sec flight velocity. Thus, the problem of providing chemical kinetic simulation must be solved, and the success of any MHD facility must be judged to a large extent by how close it meets this requirement.

The problem of what flow must be produced by a facility to provide the correct chemical kinetic simulation is not well understood. Based on the work of Gibson (Ref. 5), it appears that the free-stream velocity must be reproduced; Mach number is not too important if it is sufficiently high. The free-stream dissociation level should be sufficiently low so that the energy in dissociation is small compared to the total free-stream energy; also the free-stream dissociation should be small compared to the maximum dissociation fraction in the flow over the body. Binary scaling, keeping ρL = const where L is the characteristic body length, is possible; however, this offers little aid since high density flows are difficult to obtain in hypervelocity test facilities. Also, three-body recombination becomes important at low altitude (high density) so that the scaling law breaks down in the very place one would like to use it.

Thus, to simulate the hypervelocity flight conditions, one must provide (a) the correct free-stream velocity, (b) the correct free-stream density on a large scale model, (c) a hypersonic Mach number, (d) a low free-stream dissociation level, and (e) sufficient test time to accomplish the test objective. The first two conditions are rather specific; the last three are rather vague and depend to a large extent on the particular test. Since the flow Mach number and density level can be easily changed by a simple nozzle expansion, the proper comparison of facilities is velocity and entropy, or more precisely, total enthalpy and entropy. This comparison will be used here for the most part.

2.2 REQUIREMENT FOR SEED

Fundamental to the operation of any MHD device is that the fluid be an electrical conductor. At sufficiently high temperatures, gases become electrical conductors; the required temperature can be significantly reduced by the addition of a small amount of seed material such as potassium or cesium. This effect is illustrated in Fig. 1, which shows the equilibrium electrical conductivity of nitrogen and of nitrogen plus 0.3 percent potassium by weight at atmospheric pressure, as given by

Weber and Tempelmeyer (Ref. 6). The conductivity of air is not greatly different. Also shown is the dissociation fraction ($Z^* - 1$) for air (Ref. 7) and for nitrogen (Ref. 8). A conductivity of between 100 and 300 mho/m is normally required for accelerator operation; thus, the flow would be approximately 50 percent dissociated if pure air or nitrogen were used, whereas only about 6 percent of the air and practically no nitrogen would be dissociated if potassium seed were used. An examination of the chemical reaction rates shows that the flow is in equilibrium within the accelerators considered in this report and is frozen in any post-accelerator expansion so that the dissociation fraction in the accelerator will appear in the test section. If the test gas is accelerated, the choice is then essentially to accept a seed material or a large dissociation fraction in the test section.

2.3 EFFECT OF SEED

If a seed material is used, its effect on the test flow must be considered. Clearly, the stream bulk thermodynamic properties can change but little for a seeding fraction of 1/4 percent, typical of accelerator operation. The primary effects to be considered are the effects of increased electron concentration and increased radiation.

Electron concentrations in the stagnation region of a body with flight conditions of 23,000 ft/sec at 150,000 ft altitude and of 36,000 ft/sec at 200,000 ft altitude have been computed by Eschenroeder, et al. (Ref. 9) and are shown in Fig. 2. A potassium mass seeding fraction of 1/4 percent with all the potassium singly ionized* would yield an electron concentration of 1.85×10^{-3} mole/original mole (neglecting the coupling effect between potassium and air ionization). This value is also shown in Fig. 2 and is an upper limit for the change in electron concentration caused by the potassium. It is seen that at the 36,000 ft/sec condition the electron concentration is essentially that due to the air everywhere except very near the shock front; in fact, at the stagnation point less than 1 percent of the electrons are caused by the potassium. At the 23,000-ft/sec condition, the potassium and air contribute comparable electron concentrations. The 36,000-ft/sec stagnation flow at 200,000 ft altitude can be related to 350,000 ft altitude by binary scaling; here it is found that again the potassium and air contribute comparable electron concentrations. It is thus concluded that at high velocities and moderate

*Double ionization will not occur since the second ionization potential of potassium is 31.7 ev; this can be compared to the first ionization potential of 9.5 ev for NO and 15.5 ev for N_2.

altitudes the electron concentration near the body will be dominated by air reactions, while at low velocities and/or very high altitudes the potassium reactions will dominate.

In the region where the potassium dominates the electron concentration, the convective heat-transfer rate could be expected not to change since the electron concentration of 1.85×10^{-3} mole/original mole is less than the level indicated by Hoshizaki (Ref. 10) required to change the convective heat-transfer rate.

At high velocities the radiation heat transfer to a vehicle can be comparable to or even greater than convective heat transfer, so the potassium radiation must be considered. The equilibrium and nonequilibrium radiation about a vehicle with flight conditions of 35,000 ft/sec and 200,000 ft altitude have been computed by Allen, et al. (Ref. 11) and are shown in Fig. 3 for the stagnation streamline. In the region near the body, the gas is essentially in equilibrium, and the radiation caused by potassium transitions from the first excited state to ground level was computed and is shown in Fig. 3 (equilibrium region) to be much less than the air radiation. This results essentially from the low fraction of un-ionized potassium at these temperatures and the high first excitation potential for singly ionized potassium. Near the shock wave, the gas translational temperature is very high since the energy has not had time to go into the gas dissociation and ionization modes. Here the electron concentration is dominated by the potassium, and bremsstrahlung radiation could be important. However, an upper bound is obtained by assuming all the potassium is singly ionized and the electron temperature to be the same as the gas temperature; the value obtained was 10^{-3} watts/cc-2π-ster and is not shown in Fig. 3 since it is so much less than the air radiation. Other radiation could be important which is more difficult to estimate; for example, if the un-ionized potassium lower electronic excitation levels were excited at the gas temperature for some time before ionization could occur, rather high radiation levels would result. An estimate of this effect was obtained by computing the first resonant line radiation assuming 10 percent of the potassium atoms are in the first excited state. This value, which is probably high, is shown in Fig. 3 as the peak of the estimated potassium line radiation. Thus, it appears that the air radiation will dominate over the potassium radiation under flow conditions where radiation heat transfer is important.

There exists a possibility that the seed material will catalyze the air chemical reactions. This cannot be answered without experiments; however, the possibility is thought to be small since in the flight range of interest the reactions are mainly dissociative where catalysis is normally unimportant. This is even more true at high velocities (36,000 ft/sec)

where the stagnation point temperatures are so high that one-step dissociation of nitrogen as well as oxygen is possible.

Based on the above, it is concluded that an accelerator which obtains electrical conductivity by using a seed material is promising, whereas an accelerator not using seed will have limited utility for aerodynamic testing because of the high dissociation fraction.

3.0 TYPES OF ACCELERATORS

Various types of MHD accelerators have been proposed for re-entry testing and are applicable to widely differing flow densities. Some estimates of the flow conditions appropriate to the various configurations will be made in this section.

3.1 FARADAY ACCELERATOR

The simplest MHD accelerator concept is what is sometimes referred to as the Faraday type. This is analogous to the d-c electrical motor and is shown schematically in Fig. 4a. A magnetic field is applied across the channel, and an electric field is applied perpendicular to this. The resulting current gives rise to a JxB force which accelerates the flow. At values of the Hall coefficient $\omega\tau$ greater than unity, there will be a sizable current component in the ExB direction (flow direction) unless the electrodes are segmented and each set powered separately.

It is shown in Section 4.0 that the channel length for this type of accelerator can be written approximately as

$$L \approx \left(\frac{\rho u}{\sigma B^2}\right) \frac{u_2^2}{T\Delta S} \tag{1}$$

where u_2 is the exit velocity and ΔS is the entropy rise through the accelerator; all other terms are to be some average values. The term $[(\rho u)/(\sigma B^2)]$ has the dimension of length and is referred to as the interaction length. Keeping the accelerator length reasonable is always a problem. Equation (1) says this is accomplished by having the density ρ small; however, this would give a large Hall coefficient $\omega\tau$. In our range of interest, $\omega\tau$ is given approximately by (Ref. 6):

$$\omega\tau \approx \frac{B}{7\rho} \tag{2}$$

where B is in weber/m^2 and ρ is in kg/m^3. The interaction length can then be written approximately as

$$\frac{\rho u}{\sigma B^2} \approx \frac{u}{49 \sigma \rho (\omega\tau)^2} \tag{3}$$

Thus, the density level which will minimize the interaction length is found by using the largest possible magnetic field B and largest possible Hall coefficient $\omega\tau$ in Eq. (3).

Using B = 10 weber/m^2 and $\omega\tau$ = 10, a value of ρ = 0.14 kg/m^3 is found from Eq. (3) as the density level in the accelerator. At low velocities, approximately this value will be found at the accelerator exit; at high velocities the large entropy rise through the accelerator will lower the density at the exit by a factor of about 10. Also, an expansion ratio of about 10 is normally required between the accelerator and the test section to obtain a hypersonic Mach number. The resulting density levels are shown in Fig. 5 as the lower altitude limit for Faraday accelerators. This line is obtained more accurately in Section 5.0; however, this serves to illustrate the physical reasons for the limit.

Low densities in the test section can be obtained by increasing the post-accelerator expansion ratio from the 10 assumed above to about 10^3; an expansion ratio larger than this would give unreasonably small accelerator channel areas. In addition to this, the density level in the accelerator could be reduced by perhaps a factor 10 for high velocities and a factor of 10^2 at low velocities. This gives a total reduction in density by a factor of 10^4 at low velocities and 10^3 at high velocities, and is shown in Fig. 5 as the high-altitude Faraday accelerator limit.

It should be noted that the correct flight Mach number will be produced in the test section for the high-altitude portion of the accelerator operation indicated in Fig. 5; at the low altitudes, the post-accelerator expansion is smaller, and the Mach number will be lower than in flight.

3.2 HALL CURRENT ACCELERATOR

At values of the Hall coefficient greater than unity (low densities), the largest component of the current is in the ExB direction. Therefore, one is led to an accelerator configuration where the voltage is applied in the axial (flow) direction and produces a current perpendicular to the channel as well as in the flow direction. The electrodes are then shorted as shown in Fig. 4b. Other configurations are being considered for propulsion applications (i. e., Refs. 12 and 13); however, this configuration will serve for the order of magnitude estimates in this report.

The current components for the configuration here are given by Weber and Tempelmeyer (Ref. 6) as

$$j_y = \frac{\sigma E_H}{\omega\tau(1 + \phi^2)}\left[1 - \phi\beta_H\right] \tag{4}$$

$$j_x = \frac{\sigma E_H}{\omega\tau(1 + \phi^2)}\left[\phi + \beta_H\right] \tag{5}$$

where

$$\beta_H = \frac{uB}{E_H} \tag{6}$$

$$\phi = \frac{1 + b}{\omega\tau} \tag{7}$$

$$b = 2(1 - \alpha)^2\,\omega\tau(\omega\tau)_I \tag{8}$$

Here b is the usual ion-slip parameter, $\omega\tau$ is the Hall coefficient for electrons, $(\omega\tau)_I$ is the Hall coefficient for ions, and α is the ionization fraction.

An efficiency of the energy addition process can be defined as

$$\eta = \frac{\text{kinetic energy addition}}{\text{total energy addition}} = \frac{j_y\,uB}{j_x\,E_H} = \frac{\beta_H\left[1 - \phi\beta_H\right]}{\beta_H + \phi} \tag{9}$$

By varying E_H and thus β_H, it is found that η has a maximum value when β_H is given by

$$\beta_H = \sqrt{1 + \phi^2} - \phi \tag{10}$$

and the value of η is

$$\eta = 1 - 2\phi\left[\sqrt{1 + \phi^2} - \phi\right] \tag{11}$$

It is desirable to have η as close to unity as possible; this is accomplished by having ϕ as small as possible. By varying B, ϕ is a minimum when b = 1 so that the maximum possible conversion efficiency is approximately

$$\eta_{max} = 1 - \frac{4}{\omega\tau}$$

where the magnetic field has been picked such that

$$2(1 - \alpha)^2\,\omega\tau(\omega\tau)_I = 1$$

For seeded air at the conditions of interest,

$$\frac{(\omega\tau)_I}{\omega\tau} \approx 10^{-3}$$

which means that $\omega\tau$ should be

$$\omega\tau \approx 23$$

and the maximum conversion efficiency is

$$\eta_{max} \approx 0.83$$

To be useful, the Hall accelerator must operate near this maximum attainable conversion efficiency. For B = 10 weber/m^2 the density level in the accelerator is then approximately 0.06 kg/m^3.

An important characteristic of a Hall current accelerator is demonstrated here; namely, there is a fundamental upper limit to the conversion efficiency that can be attained. For a Faraday accelerator operating with no Hall currents, the conversion efficiency is

$$\eta = \frac{j_y \, u \, B}{j_y \, E_y} = \frac{u \, B}{E_y} = \beta \tag{12}$$

which can, in principle at least, be made as near unity as desired by proper choice of the applied E field. If E in the Faraday accelerator is picked to give the same body force term as in the Hall accelerator, that is, j_y's set equal, it is found that

$$\frac{1 - \beta}{\beta} \approx \phi$$

which is a conversion efficiency of 0.92 for the Faraday accelerator compared to the 0.83 for the Hall accelerator. This indicates that the entropy rise in the Hall accelerator will be about double that of the Faraday accelerator.

Allowing for a density decrease through the Hall accelerator by a factor of 10 associated with the large entropy rise and a post-accelerator expansion ratio of 10, the maximum density level for a Hall accelerator at low velocities is then about 6×10^{-4} kg/m^3. At high velocities, the density will decrease another factor of 10 because of increased entropy rise. These values are shown in Fig. 5 as the low-altitude limit of the Hall accelerator.

The lower density limit of the Hall accelerator is not clear. It appears that the magnetic field could be reduced by a factor of 10 and the density within the accelerator by a factor of 10^2; sufficient interaction would be retained since E_H would be much larger than the value which was used to maximize the conversion efficiency, Eq. (10). A larger entropy rise would then reduce the accelerator exit density another factor of 10 for a total reduction of 10^3. This value is shown in Fig. 5 as the high-altitude limit for a Hall accelerator.

3.3 TRAVELING-WAVE ACCELERATOR

In an induction electric motor, the torque is produced by the interaction of the applied magnetic field with the currents induced in the rotor by the effective motion of this same applied magnetic field. Similar to

this, one can have an accelerator where the magnetic field is varied in time such as to produce wave motion, that is, traveling waves in the flow direction. This will induce currents in the gas such that the interaction will effectively drag the flow with the traveling magnetic field. This type of accelerator is shown schematically in Fig. 4c. Other configurations which have some important advantages have been considered (i. e., Refs. 4 and 15); however, this configuration will serve our purposes here.

Fundamental to this accelerator is that the gas must be contained in the magnetic field waves. This requires that the flow dynamic pressure be much less than the magnetic pressure:

$$\frac{\rho u^2}{B^2/\mu} << 1$$

The magnetic field coils tend to cancel each other, and it is difficult to have effective field strengths greater than say 0.3 w/m^2. Using this field strength and placing the above pressure ratio at 0.1, the density level is found to be about 10^{-4} kg/m^3. Allowing for a density decrease through the accelerator and some expansion at the exit, the value of 10^{-4} will be reduced to say 10^{-6}, which is shown in Fig. 5 as the low-altitude limit for traveling-wave accelerators at moderate velocities.

The low-density limit for a traveling-wave accelerator will correspond to the point where there are too few collisions to accelerate the neutral particles. This will permit about another factor of 10^2 reduction in density level and is shown in Fig. 5 as the high-altitude limit for traveling-wave accelerators.

3.4 ELECTROSTATIC ACCELERATOR

An accelerator for producing high-velocity free-molecule flow of a neutral-particle stream was proposed by Cann, et al. (Ref. 16) and is shown schematically in Fig. 4d. It consists essentially of an ion-engine type accelerator to obtain a high-speed ion beam. The high-speed ions are then neutralized by crossing the beam with a low-speed neutral particle beam and utilizing resonant charge exchange. The cross section for resonant charge exchange (that is, transferring an electron between molecules or atoms of the same element) is much larger than for momentum transfer, ionization, dissociation, etc. This is fundamental to the technique and allows the production of a high-velocity neutral beam utilizing electrostatic acceleration.

The low-altitude limit corresponds to space charge limits for the ion accelerator. Order of magnitude limits for this technique were

made in Ref. 16 and are over 500,000 ft altitude and hence not shown in Fig. 5.

3.5 ACCELERATORS FOR AERODYNAMIC TESTING

The accelerator estimates given in Fig. 5 should be considered as a maximum range of values because other constrains may be of prime importance. For example, energy storage and/or power limitations will be of prime importance at low altitudes. Also, smaller magnetic fields will be available for a continuous facility, and heat transfer could be severe. Thus, the low altitude limits for the Faraday and Hall accelerators in Fig. 5 must be raised for continuous facilities. Also, they will be raised if the correct free-stream Mach number is required.

Based on the above order of magnitude estimates, it appears that only the Faraday accelerator and the Hall accelerator are of interest for aerodynamic testing in the altitude range from 100,000 to 300,000 ft, where most of the flight problems occur. Further, the Hall accelerator will be limited to rather high-altitude conditions, and the Faraday accelerator will be the most useful for practical aerodynamic testing. Therefore, consideration in this report will be limited from here on to the Faraday accelerator.

4.0 FARADAY ACCELERATOR SCALING LAWS

4.1 CHANNEL LENGTH

The required channel length is of prime importance in MHD accelerator work. Essentially one would like to have the channel very long to have an efficient acceleration process (inviscid analysis); however, this would lead to very thick viscous boundary layers which could even dominate the entire accelerator flow. Therefore, an estimate of the accelerator channel length will be made first. Consideration will be limited to a Hall-current neutralized accelerator.

It was shown in Eq. (12) that of the total energy added to the flow, the fraction β goes in as kinetic energy which leaves the fraction $(1 - \beta)$ as thermal energy addition. Therefore, the entropy rise can be written as

$$T\,dS = (1 - \beta)\,dH \tag{13}$$

where H is the total enthalpy of the flow,

$$H = \frac{u^2}{2} + h$$

A total energy equation can be written as

$$\rho u \frac{dH}{dx} = j_y E_y \tag{14}$$

or

$$dx = \frac{\beta^2 \rho}{(1-\beta)\sigma B^2 u} dH \tag{15}$$

Normally the change in static enthalpy h is small so $dH \approx u\, du$; also β will be near unity. Thus, Eqs. (13) and (15) are combined to give

$$L \approx \left(\frac{\rho u}{\sigma B^2}\right) \frac{(\Delta u)^2}{T \Delta S} \tag{16}$$

For a high-performance accelerator, $\Delta u \approx u_2$, the exit velocity. The entropy rise ΔS can be thought of as density decrease or channel area increase and is limited to $\Delta S/R$ about 3 to 4. The conductivity varies approximately as

$$\sigma \backsim (Z^* - 1)\sqrt{\theta} \tag{17}$$

so the length varies as

$$L \backsim \frac{\rho u^3}{(Z^* - 1)\sqrt{\theta}\, B^2 T \Delta S} \backsim \frac{u^3}{(Z^* - 1)\sqrt{\theta}\, \rho (\omega r)^2 T \Delta S} \tag{18}$$

where $(Z^* - 1)$ is the gas dissociation level and θ is the mass seeding fraction.

4.2 ACCELERATOR SCALING LAWS

The channel length itself is often not as critical as the channel length-to-diameter ratio; this is a measure of the severity of the boundary-layer growth and can be expressed as

$$\frac{L}{D} = \frac{L}{\sqrt{A}} = \frac{L\sqrt{\rho u}}{\sqrt{\dot{m}}} \tag{19}$$

where $\dot{m}$ is the mass flow. The mass flow can be expressed in terms of total power P and the exit total enthalpy; then Eqs. (18) and (19) are combined to give

$$\frac{L}{\sqrt{A}} \backsim \frac{u^{4.5}}{(Z^* - 1)\sqrt{\theta \rho P}\, (\omega r)^2 T \Delta S} \tag{20}$$

Since the maximum value of $L/\sqrt{A}$ is a rather firm limit, Eq. (20) can be considered an expression to estimate the increase in velocity which can be obtained by changing various quantities. For example, doubling the dissociation fraction will increase the velocity u by 17 percent;

doubling θ increases u by only 8 percent. To double u requires the power P be increased by a factor 10^3; this also points out that there is a minimum power level below which a Faraday accelerator should not be considered.

4.3 HALL VOLTAGE

The Hall potential in a Hall current neutralized accelerator is given by (Ref. 6)

$$E_H = \frac{j_y B}{n_e e} \tag{21}$$

This can be combined with the energy Eq. (14) to give

$$E_H \, dx = \frac{\beta \, m_n}{\alpha \, e} \, dH$$

where m_n is the mass of the neutral particles and the ionization fraction α is small. Assuming β and α are approximately constant, this is integrated to give the total Hall voltage as

$$V_H = 1.5 \times 10^{-7} \frac{\beta u^2}{\alpha} \tag{22}$$

where V_H is in volts, u is in m/sec, and the constant has been evaluated for air. The accelerator exit velocity has been assumed large compared to the inlet velocity.

Voltages computed from Eq. (22) are shown in Fig. 6. For $\beta/\alpha = 1000$, typical of the accelerators considered here, a Hall voltage of 15,000 volts is required to obtain 10,000 m/sec. This serves to illustrate the rather high axial voltages which are characteristic of a high-performance Faraday accelerator and which give rise to finely segmented electrodes and severe insulation problems between electrodes.

5.0 EQUILIBRIUM ACCELERATOR PERFORMANCE

5.1 OPTIMUM ACCELERATOR SOLUTIONS

The selection of a MHD accelerator design to produce specified test section conditions is complicated by the large number of parameters involved. Referring to Fig. 7, one must choose the operating conditions H_o and S_o for the gas supply, the channel inlet conditions, the channel area distribution A(x), magnetic field distribution B(x), and the electric field distribution E(x). These quantities must be chosen within the

framework of appropriate physical constraints. The solution for the optimum accelerator in terms of maximum exit total enthalpy, minimum exit entropy level, or minimum channel length* was given by Ring (Ref. 17) and will be used here to estimate the Faraday accelerator performance limits. This solution includes optimum matching of accelerator to the hot gas source, real air thermodynamics, and equilibrium electrical conductivity; it will be used here in the sense of maximizing the total enthalpy with the exit entropy level and channel length fixed.

Various physical constraints are appropriate and include: (a) effective reservoir pressure and temperature limitations of the hot gas source, (b) maximum available magnetic field strength, (c) maximum value of the Hall coefficient $\omega\tau$, (d) maximum channel static pressure based on structural and/or heat-transfer limits, and (e) maximum gas dissociation level in the channel. In addition, one must assume a mass seeding fraction θ and a channel length based on boundary-layer considerations.

A large number of accelerator solutions were obtained with various assumed values of the physical constraints. All of the solutions were obtained by numerical integration of Eqs. (25), (26), and (27) of Ref. 17. The integrations were performed using the numerical curve fits given by Lewis and Burgess (Ref. 18) for the real air thermodynamics of Hilsenrath et al. (Ref. 7). The ionization fraction was found by using Saha's equation for the potassium seed; the electrical conductivity was then computed using an electron-neutral collision cross section of 10^{-19} m^2 and the Spitzer value for the electron-ion collision cross section.

5.2 EXAMPLE ACCELERATOR SOLUTIONS

The details of two of the optimum accelerator solutions obtained are shown in Figs. 8 and 9 for a continuous and a short duration accelerator, respectively.

The continuous accelerator (Fig. 8) is assumed to be supplied by an arc heater at 100 atm pressure, typical of current high-pressure arc heaters. The reservoir temperature of 4750°K should not be considered specified but rather the optimum value corresponding to a specified exit entropy value of S/R = 35.16 and a length of 4 m. The channel static pressure was limited to 10 atm for heat-transfer considerations. The maximum value of Z* was taken as 1.06, and a maximum magnetic field

---

*It should be noted that, as shown by Ring (Ref. 17), these three distinct optimization problems lead to the same solution.

was taken as B = 4 w/m^2, which could be operated continuously. The Hall coefficient $\omega\tau$ was limited to 5 and the potassium mass seeding rate was taken as 0.25 percent.

The pressure in the channel initially remained constant (Fig. 8a) at 10 atm while the temperature increased until the dissociation limit was reached. The pressure and temperature then both decreased along a line of $Z^* = 1.06$ while $\omega\tau$ increases to its limit of 5. The Hall coefficient $\omega\tau$ then remains constant while the pressure and magnetic field decrease. The velocity and Mach number (Fig. 8b) increased nearly linearly down the channel. The rapid increase in area near the channel exit is characteristic of a solution where $\omega\tau$ is constant.

The short duration accelerator (Fig. 9) has an effective reservoir pressure of 10,000 atm. This value is typical of the conditions which can be obtained from a shock tunnel operating in the nonreflected mode. Again, the effective reservoir temperature of 10,250°K is not specified but rather is the optimum value corresponding to a specified exit entropy S/R = 34.83 and a channel length of 4 m. The constraints are the same as the previous case, except that the magnetic field has been increased to 10 w/m^2, which can be obtained with a pulsed magnet, and no limit has been placed on the static pressure since the values obtained are not excessive for a pulsed device.

The general characteristics of this solution are similar to the previous case.

5.3 ACCELERATOR PERFORMANCE LIMITS

Having obtained a number of optimum accelerator solutions, a plot can be made of accelerator exit total enthalpy as a function of exit entropy level. This has been done for a continuous accelerator in Fig. 10 as a Mollier diagram overlay and shows the effect of length, maximum Hall coefficient, and reservoir pressure. The corresponding optimum arc-heater entropy levels $(S/R)_o$ have been indicated at several points along each curve. Since these limit lines correspond to optimum accelerator solutions, they are to be considered as absolute accelerator limits in the sense that it is impossible for any other accelerator to have higher performance (that is, higher total enthalpy at the same entropy) within the assumed system of constraints. Clearly, higher performance can be obtained by relaxing any of the assumed constraints.

For reference, a scale of total enthalpy in terms of equivalent velocity has been included. Also, equivalent altitudes for duplication of

atmospheric density and temperature are indicated based on the assumption that both chemical reactions and vibration are frozen in the post-accelerator expansion. This assumption should be valid above $S/R \approx 35$ but somewhat in error below this.

A moderate gain in performance is obtained by increasing the Hall coefficient or the accelerator channel length. The effect of increasing the arc-heater pressure from 100 to 200 atm together with an increase in the channel static pressure limit from 10 to 100 atm is seen to be quite small. This minor gain in performance does not appear to justify the associated severe heat-transfer problems. Also, it is found that $(S/R)_o$ can be changed substantially from the optimum values indicated on the curves with only a minor loss of performance.

Since the limiting accelerator performance depends only weakly on the reservoir pressure, a single line can effectively represent the limiting accelerator performance for each type of hot gas supply. Figure 11 shows the accelerator performance limits for 100, 1000, and 10,000 atm effective reservoir pressure. The 100-atm line represents arc heaters with continuous accelerators; as such, the magnetic field is limited to 4 w/m^2 and channel static pressure to 10 atm. The 1000-atm line represents a short duration accelerator using a reflected shock tunnel as the gas source; a magnetic field of 10 w/m^2 and a static pressure limit of 600 atm were used. It should be noted that this high static pressure was realized only in accelerators with an exit velocity below 28,000 ft/sec. The 10,000-atm line represents a short duration accelerator using a non-reflected shock tunnel as the gas source; the magnetic field was limited to 10 w/m^2 and that static pressure to 1000 atm. Again the high pressure was realized only for accelerator exit velocities less than 22,000 ft/sec.

These calculations show two important facts. First, there is a rather well-defined limit in the maximum velocity which can be obtained under a given set of physical constraints. Second, the entropy levels (and thus density level) depend only weakly on the type of gas source used for a high-performance accelerator; increasing the gas source pressure level by a factor of 10 increases the test section density only by about 50 percent.

The limiting performance lines obtained can be scaled with reasonable accuracy using Eqs. (18) or (20). However, it takes large changes in say Z^* or mass seeding fraction θ to change the performance significantly. A Hall coefficient of 5 should present no major difficulties; a value of 10 may produce severe problems. Therefore, the limiting lines shown in Fig. 11 can be considered, for practical purposes, the upper performance limits of Faraday accelerators using equilibrium electrical conductivity.

6.0 NONEQUILIBRIUM ACCELERATOR

6.1 NONEQUILIBRIUM ELECTRON TEMPERATURE

When an electric field is applied to a plasma, the electrons start to drift while the ions remain relatively immobile because of their large mass. Since the electrons are falling through a potential, energy is added to the electrons, and they will be raised to a higher energy level (that is, higher temperature) than the heavy gas particles. The magnitude of the temperature difference depends on how rapidly the electron energy can be transferred to the heavy gas particles through collisions.

This effect was first proposed for MHD devices by Kerrebrock (Ref. 19) who gave the electron temperature as

$$T_e = T_g + \frac{2 m_g}{3 k \delta} \left(\frac{j}{n_e e} \right)^2 \tag{23}$$

Here m_g is the mass of the gas heavy particles, and δ is a correction factor to account for inelastic collisions of electrons with these gas particles; $\delta = 2$ corresponds to elastic collisions. The gas ionization fraction is assumed to be given by Saha's equation using the electron temperature. Fair agreement has been found between the electrical conductivity computed on the basis of this model and experiments with monatomic gases (Refs. 20 and 21). The experiments indicated a value $\delta \approx 10$; this was attributed to radiation losses.

Equation (23) has been written by Hurwitz et al. (Ref. 22) in the form

$$T_e = T_g + \frac{2 m_g}{3 k \delta} \left(\frac{1 - \beta}{\beta} \right)^2 (\omega \tau)^2 \, u^2 \tag{24}$$

Using typical values of $\beta = 0.9$, $\omega\tau = 5$, and $u = 5000$ m/sec, the electron temperature is found to be 1800°K higher than the gas temperature for $\delta = 10$; however, if $\delta = 10^3$ the 1800°K is reduced to only 18°K. This demonstrates the fundamental importance of the magnitude of δ on nonequilibrium accelerators. The magnitude of δ for air has not been established; it could be as low as 10 or as high as 10^2 to 10^3 if the electrons are effective in the excitation of say nitrogen vibration (Ref. 23). However, the electrical conductivity data obtained by Tempelmeyer, et al. (Ref. 24) in potassium seeded nitrogen indicated nonequilibrium effects with δ near 10^2.

Nonequilibrium ionization probably cannot be maintained in nondissociated air without seeding. If one were to produce nitrogen ions, the extremely fast dissociative-recombination reaction

$$N_2 + e^- \rightarrow N + N + \text{Radiation}$$

would quickly lead to a fully dissociated flow. Also, the probability of excitation of N_2 vibration by electrons will be greater at high electron temperatures; continued vibrational excitation would again lead to dissociation. Therefore, the possibility of obtaining nonequilibrium conductivity in nondissociated air appears the greatest by using a seed material such as potassium and maintaining the electron temperature in the 4000°K range.

6.2 NONEQUILIBRIUM ACCELERATOR

Assuming nonequilibrium conductivity can be obtained, there will still be limitations on accelerator performance. Equation (24) shows that nonequilibrium electron temperatures cannot be obtained if $(1 - \beta)$ is too small; Eq. (13) shows the entropy rise to be proportional to this same factor. Also, the entropy rise becomes large if the gas temperature T is too small. Based on these considerations, it is estimated that a factor of 10 increase in density at high velocities and a factor of 10^2 at low velocities could be obtained from Faraday accelerators if nonequilibrium conductivity is realized.

7.0 CONCLUSIONS

Estimates of the performance limitations of the various types of MHD accelerators indicate that only Hall accelerators and Faraday accelerators will be useful for aerodynamic test purposes, with the Hall accelerators limited to high-altitude (low-density) conditions. The lower performance of the Hall accelerator is the result of the fundamentally lower conversion efficiency when operating in the Hall mode.

It was shown that to obtain the required electrical conductivity one must either accept a highly dissociated flow or a seed material. Estimates were made of several possible effects of the seed material on the flow. It was concluded that an accelerator which uses a seed material is promising, but an accelerator not using seed will have limited utility for aerodynamic testing.

Performance estimates of a Faraday accelerator using potassium seed and equilibrium conductivity indicate that velocities over 30,000 ft/sec should be obtained from a continuous accelerator and over 40,000 ft/sec from a pulsed accelerator. To obtain this performance, the accelerator must operate near atmospheric pressure, in the 3000 to 4000°K temperature range, and at values of the Hall coefficient $\omega\tau$ greater than 5. Substantial increases in density level can probably be obtained at low

velocities (25,000 ft/sec) if nonequilibrium electrical conductivity is obtained.

REFERENCES

1. Cann, G. L. and Buhler, R. D. "A Survey and Prediction of the Performance Capability of Coaxial Arc Heaters." Paper to be presented at AGARD Specialists' Meeting on Arc Heaters and MHD Accelerators for Aerodynamic Purposes, Rhode-Saint-Genese, Belgium, September 21-23, 1964.

2. Bird, K. D., Martin, J. F., and Bell, T. J. "Recent Developments in the Use of the Hypersonic Shock Tunnel as a Research and Development Facility." Third Hypervelocity Techniques Symposium, Denver, Colorado, March 1964, p. 7.

3. Boison, J. Christopher and Ring, Leon E. "A Low Density Hypervelocity Facility for Development Testing." Presented at the Eighth Annual AFSC Science and Engineering Symposium, San Francisco, California, 3-4 October 1961.

4. Harney, D. J. "Chemical Kinetic Regimes of Hypersonic Flight Simulation." AEDC-TDR-63-3 (AD 295147), January 1963.

5. Gibson, W. E. "Dissociation Scaling for Nonequilibrium Blunt-Nose Flows." ARS Journal, Vol. 2, No. 2, February 1962.

6. Weber, R. E. and Tempelmeyer, K. E. "Calculation of the D-C Electrical Conductivity of Equilibrium Nitrogen and Argon Plasma With and Without Alkali Metal Seed." AEDC-TDR-64-119 (AD 602858), June 1964.

7. Hilsenrath, J., Klein, M., and Woolley, H. W. "Tables of Thermodynamic Properties of Air Including Dissociation and Ionization from 1,500 to 15,000°K." AEDC-TDR-59-20 (AD 229962), December 1959.

8. Hilsenrath, Joseph and Klein, Max. "Tables of Thermodynamic Properties of Nitrogen in Chemical Equilibrium Including Second Virial Corrections from 2000°K to 15,000°K." AEDC-TDR-63-162 (AD 432210), March 1964.

9. Eschenroeder, A. Q., Daiber, J. W., Golian, T. C., and Hertzberg, A. "Shock Tunnel Studies of High-Enthalpy Ionized Airflows." Paper presented at the AGARD Meeting on High Temperature Aspects of Hypersonic Fluid Dynamics, Brussels, Belgium, March 1962.

10. Hoshizaki, H. "Heat Transfer in Planetary Atmospheres at Super-Satellite Speeds." ARS Journal, Vol. 32, No. 10, October 1962, p. 1544-1552.

11. Allen, R. A., Rose, P. H., and Camm, J. C. "Nonequilibrium and Equilibrium Radiation at Super-Satellite Re-entry Velocities." AVCO-Everett Research Laboratory Report 156, September 1962.

12. Cann, Gordon L., Ziemer, Richard W., Marlotte, Gary L. "The Hall Current Plasma Accelerator." Paper presented at the ARS Electric Propulsion Conference; Colorado Springs, Colorado; March 11-13, 1963.

13. Sevier, J. R., Hess, R. V., and Brockman, P. "Coaxial Current Accelerator Operation at Forces and Efficiencies Comparable to Conventional Crossed-Field Accelerators." ARS Journal, Vol. 32, No. 1, January 1962.

14. Jones, R. E. and Palmer, R. W. "Experimental Results of a Traveling Magnetic Wave Plasma Engine." Proceedings of Fifth Symposium on the Engineering Aspects of Magnetohydrodynamics, M.I.T., April 1-2, 1964.

15. Smotrich, H., Janes, G. S., and Bratenahl, A. "Experimental Studies of a Magnetohydrodynamic C. W. Traveling Wave Accelerator." Proceedings of Fourth Symposium on the Engineering Aspects of Magnetohydrodynamics, April 10-11, 1963.

16. Cann, G. L., Teem, J. M., Buhler, R. D., and Branson, L. K. "Magnetogasdynamic Accelerator Techniques." AEDC-TDR-62-145 (AD 277954), July 1962.

17. Ring, Leon E. "Optimization of MHD Crossed-Field Accelerators and Generators." Paper presented at the Fifth Symposium on Engineering Aspects of Magnetohydrodynamics, M. I. T., April 1-2, 1964. Also AEDC-TDR-64-278 (to be published).

18. Lewis, Clark H. and Burgess, E. G., III. "Empirical Equations for the Thermodynamic Properties of Air and Nitrogen to 15,000°K." AEDC-TDR-63-138 (AD 411624), July 1963.

19. Kerrebrock, Jack L. "Conduction in Gases with Elevated Electron Temperature." Proceedings of the Second Symposium on the Engineering Aspects of Magnetohydrodynamics, University of Pennsylvania, March 9-10, 1961.

20. Kerrebrock, J. L. and Hoffman, M. A. "Experiments on Non-Equilibrium Ionization Due to Electron Heating." Presented at the 1964 AIAA Aerospace Sciences Meeting, Preprint 64-27, New York, N. Y., January 20-22, 1964.

21. Zukowski, E. E., Cool, T. A., and Gibson, E. G. "Experiments Concerning Non-Equilibrium Conductivity in a Seeded Plasma." Presented at the 1964 AIAA Aerospace Sciences Meeting, Preprint 64-28, New York, N. Y., January 20-22, 1964.

22. Hurwitz, H. Jr., Sutton, G. W., and Tamor, S. "Electron Heating in Magnetohydrodynamic Power Generators." ARS Journal, August 1962, p. 1237-1243.

23. Schultz, G. J. "Vibrational Excitation of Nitrogen by Electron Impact." Phys. Rev., Vol. 128, 1962, p. 174.

24. Tempelmeyer, K. E., Windmueller, A. K., and Rittenhouse, L. E. "Development of a Steady-Flow JxB Accelerator for Wind Tunnel Application." Paper presented at the AGARD Specialists' Meeting on Arc Heaters and MHD Accelerators for Aerodynamic Purposes, Rhode-Saint-Genese, Belgium, September 21-23, 1964. Also AEDC-TDR-64-261, December 1964.

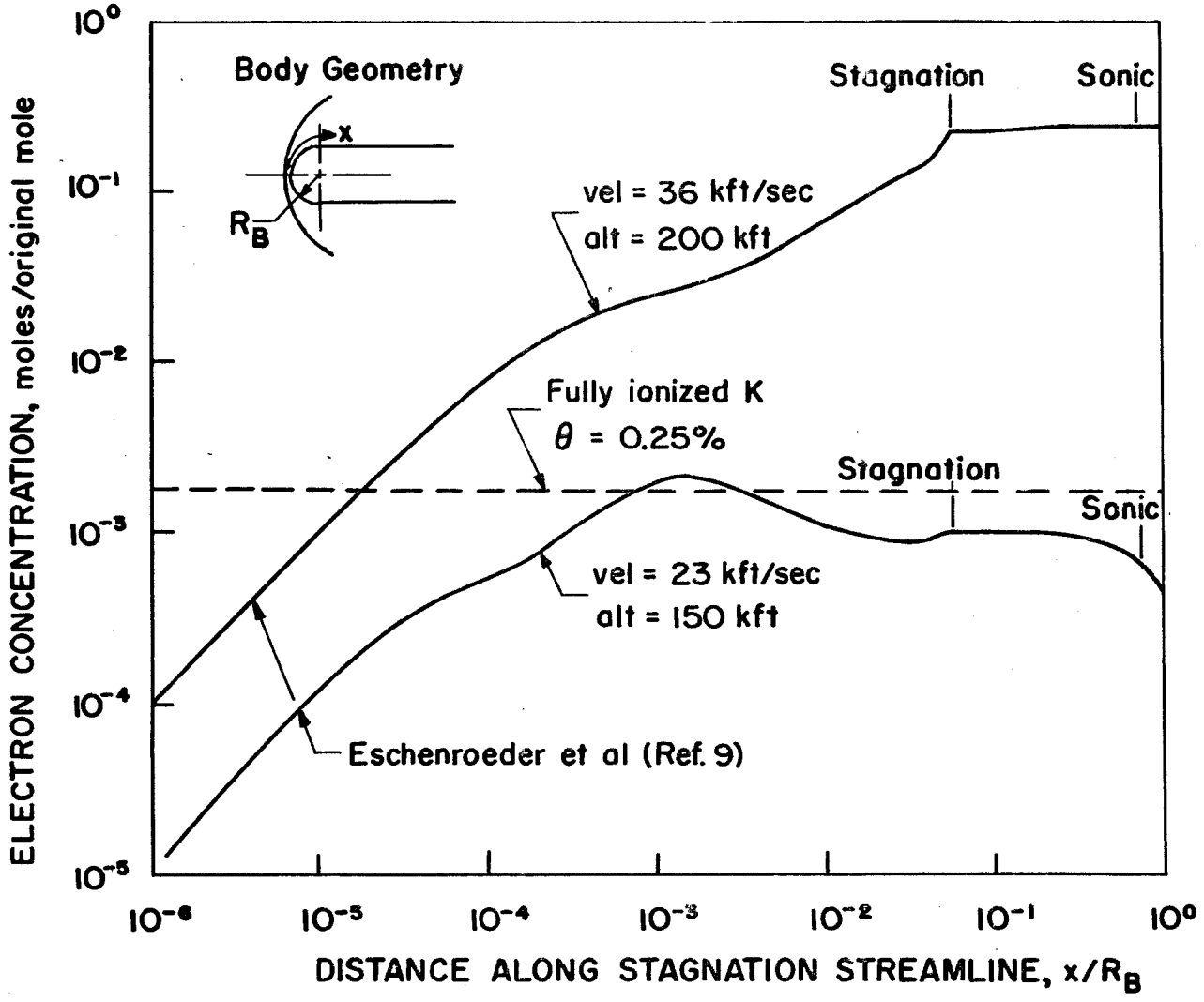

Fig. 2 Electron Concentration in Stagnation Region of Flight Vehicle and Effect of Potassium Seed

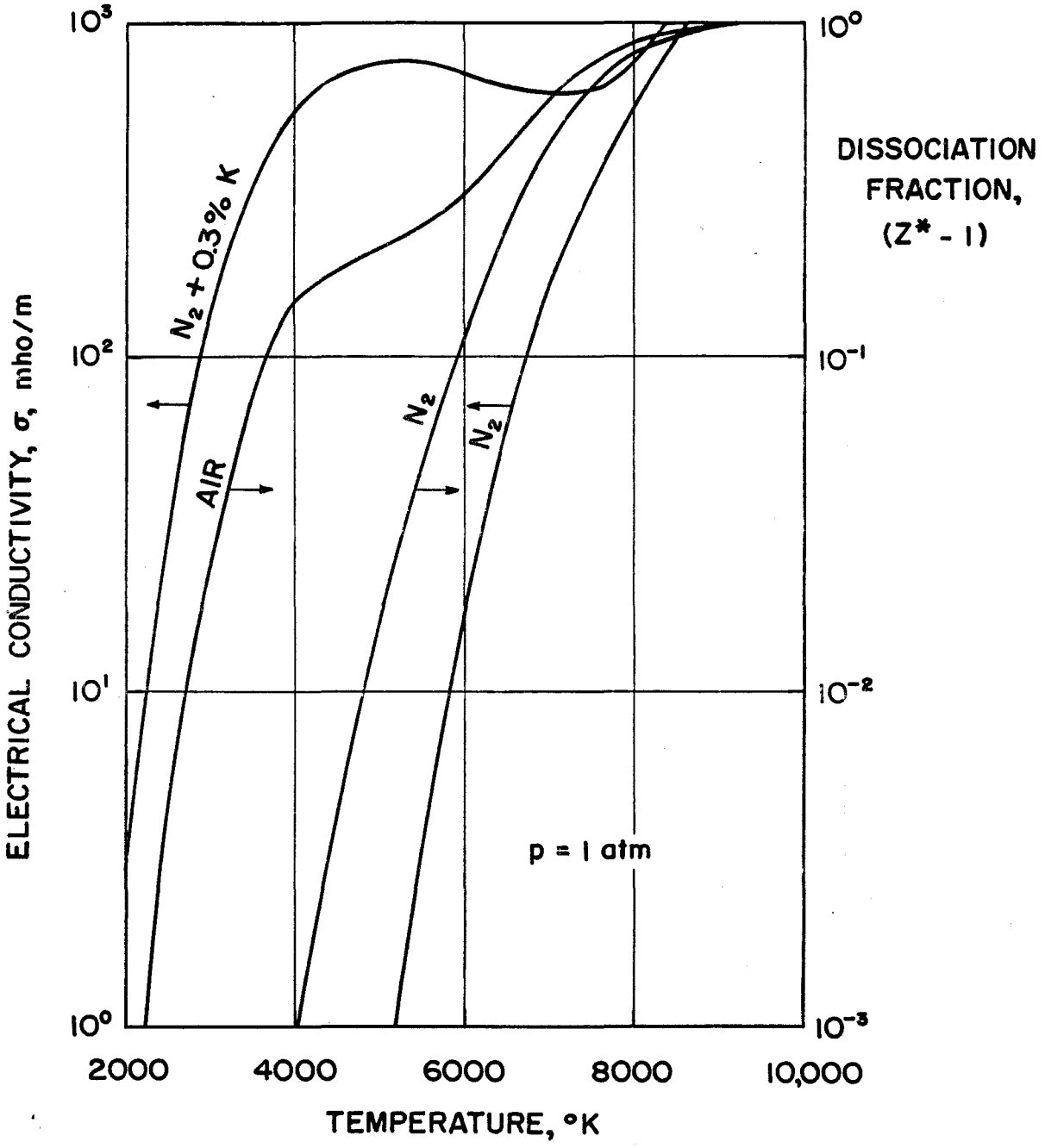

Fig. 1 Comparison of Electrical Conductivity and Dissociation Fraction, with and without Seed

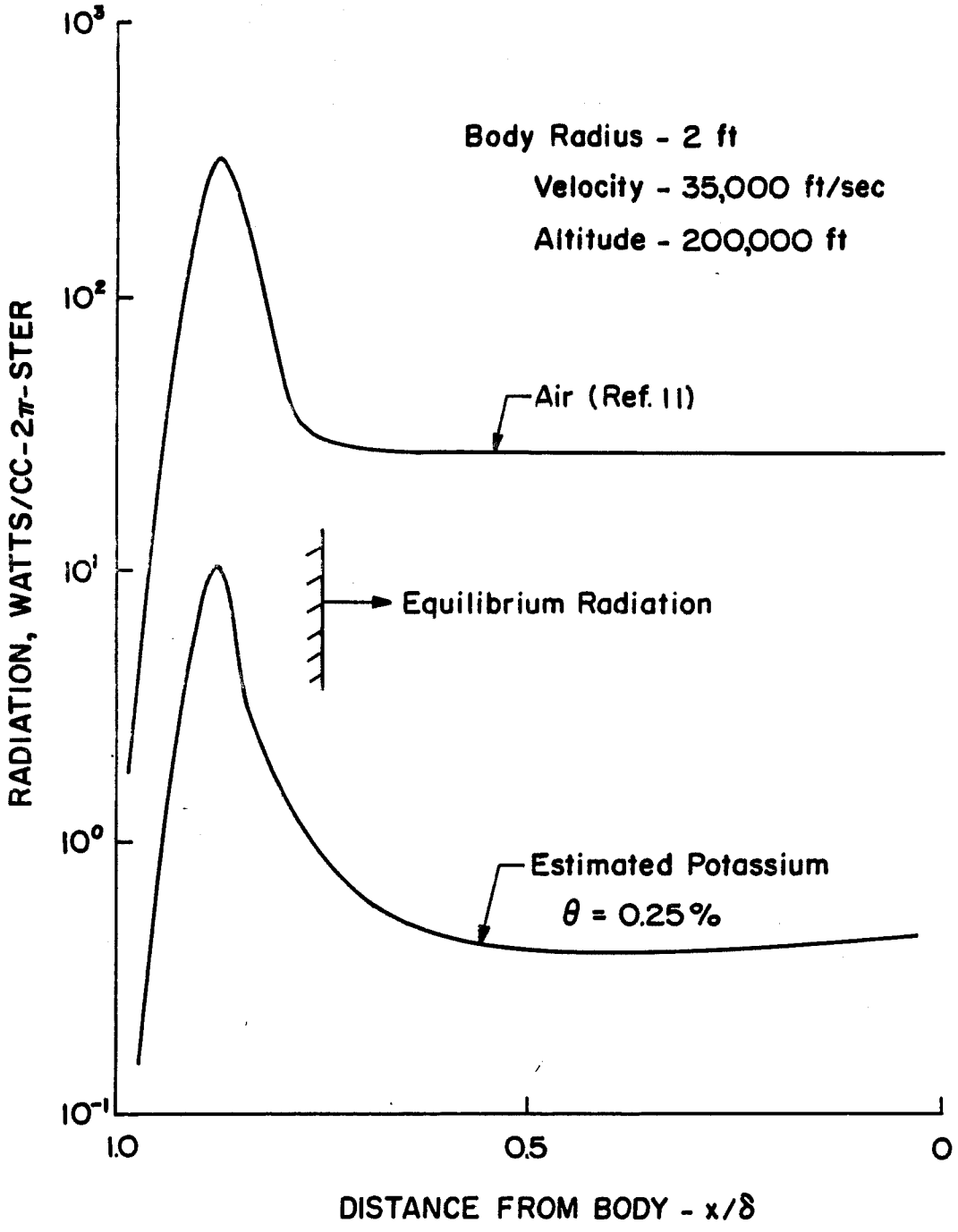

Fig. 3 Radiation in Stagnation Region for Air and Estimated for Potassium

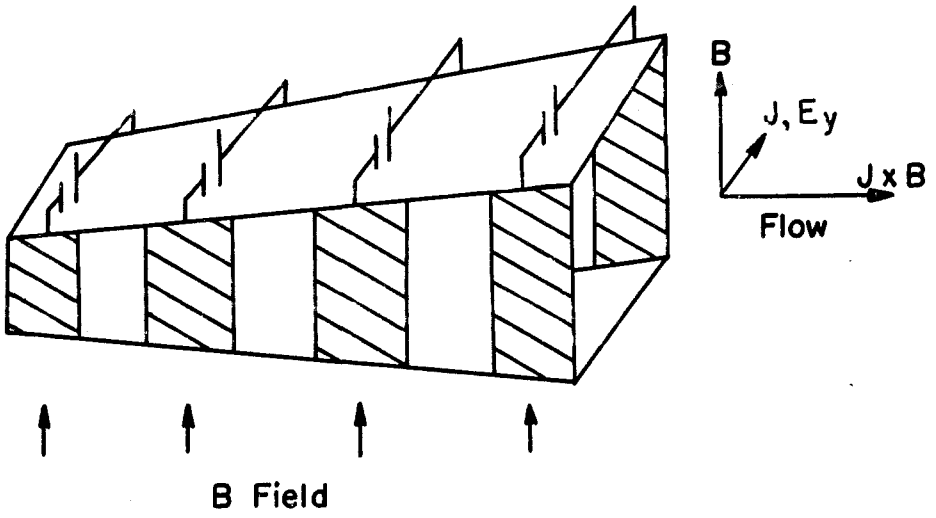

a. Faraday Accelerator

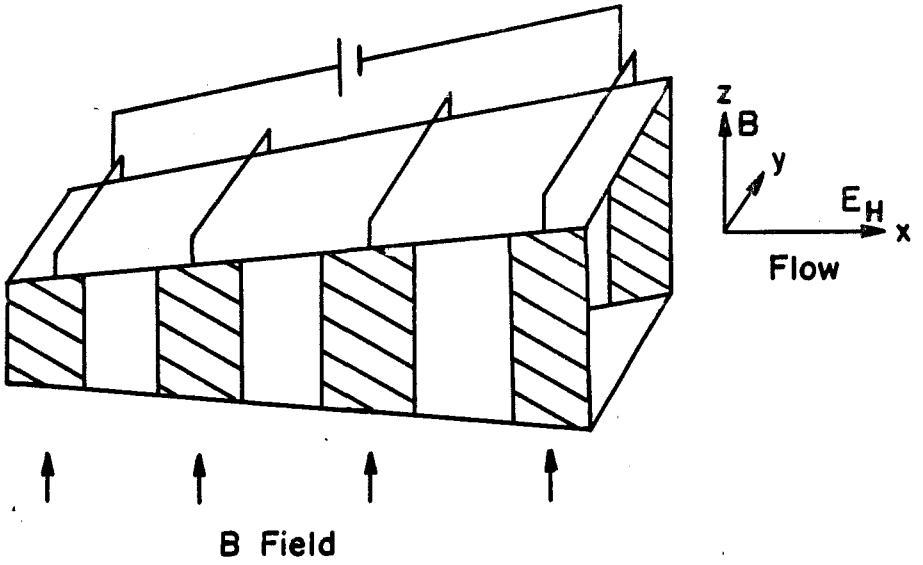

b. Hall Accelerator

Fig. 4 Accelerator Types

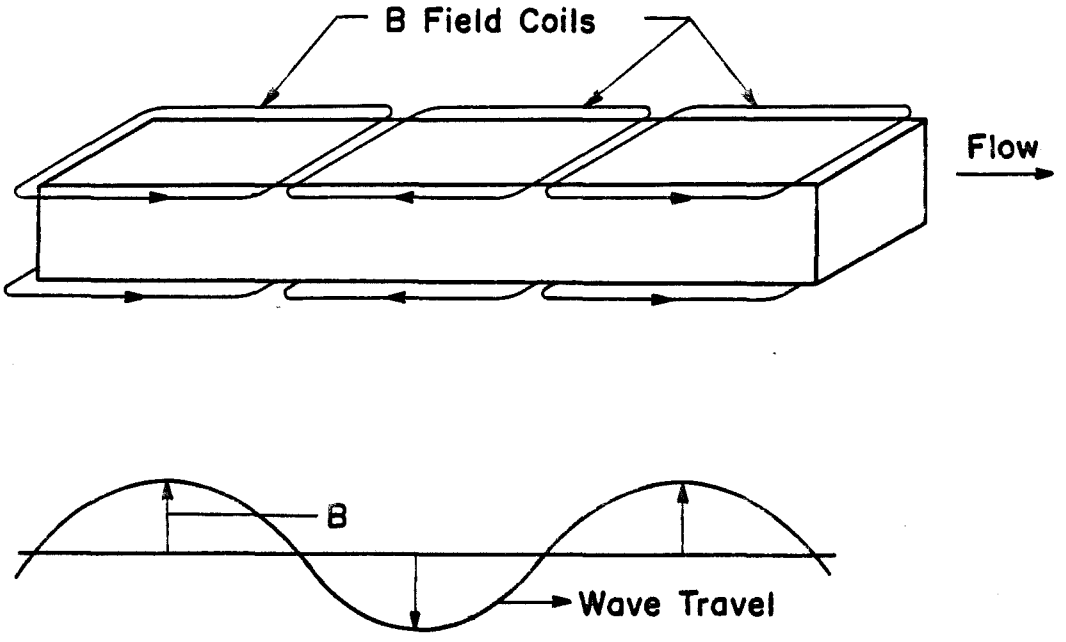

c. Traveling Wave Accelerator

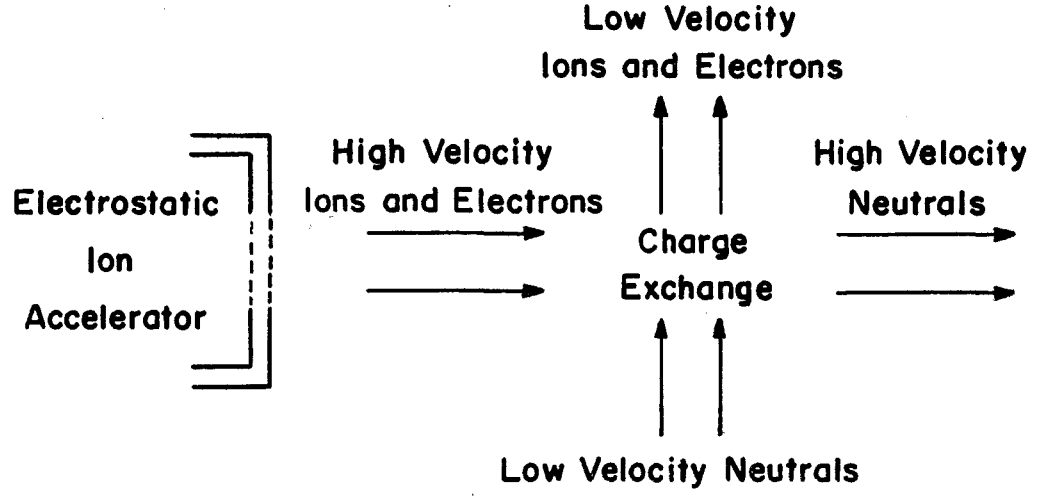

d. Electrostatic Accelerator

Fig. 4 Concluded

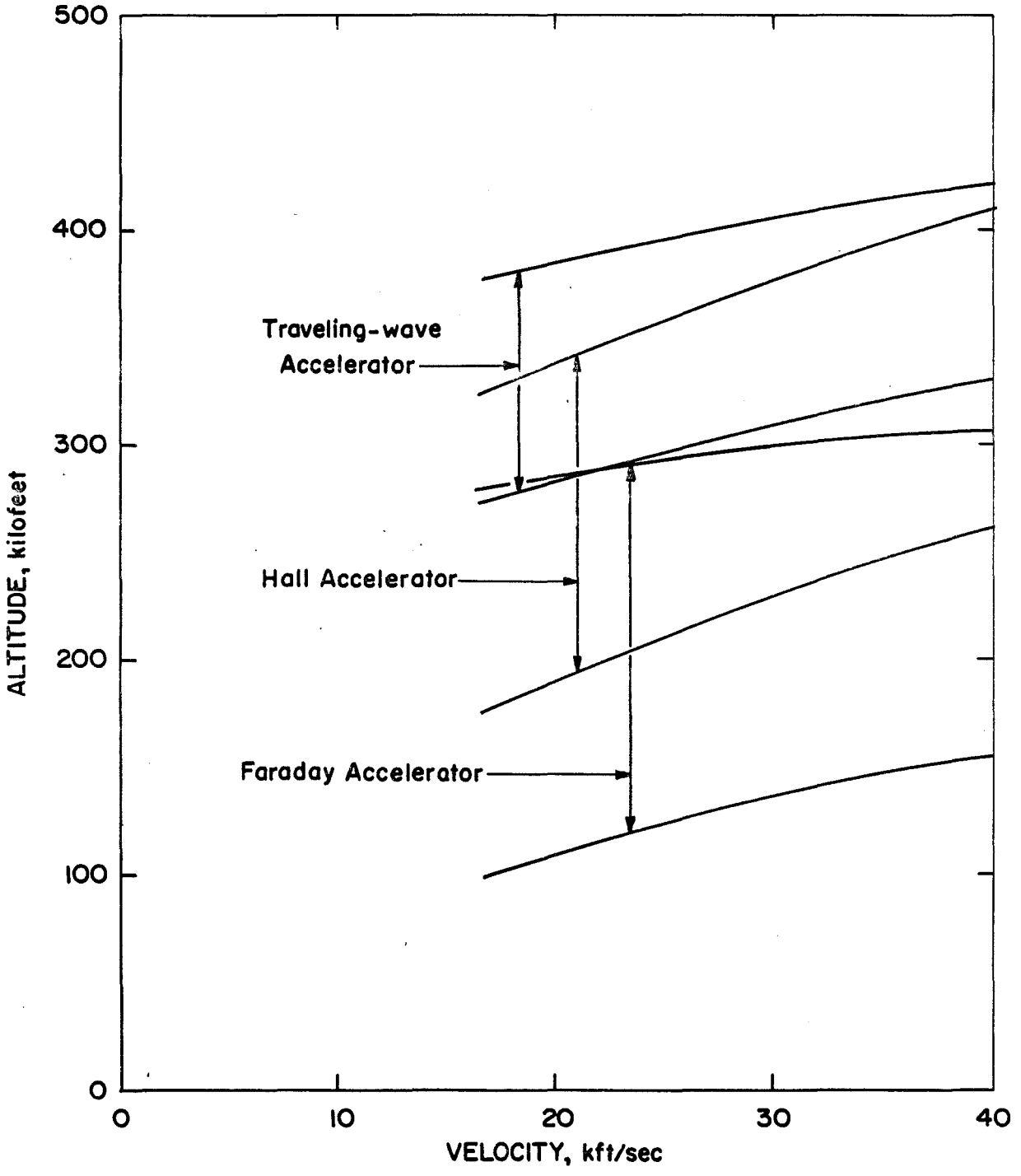

Fig. 5 Estimated MHD Accelerator Operating Range, Velocity, and Density Simulation

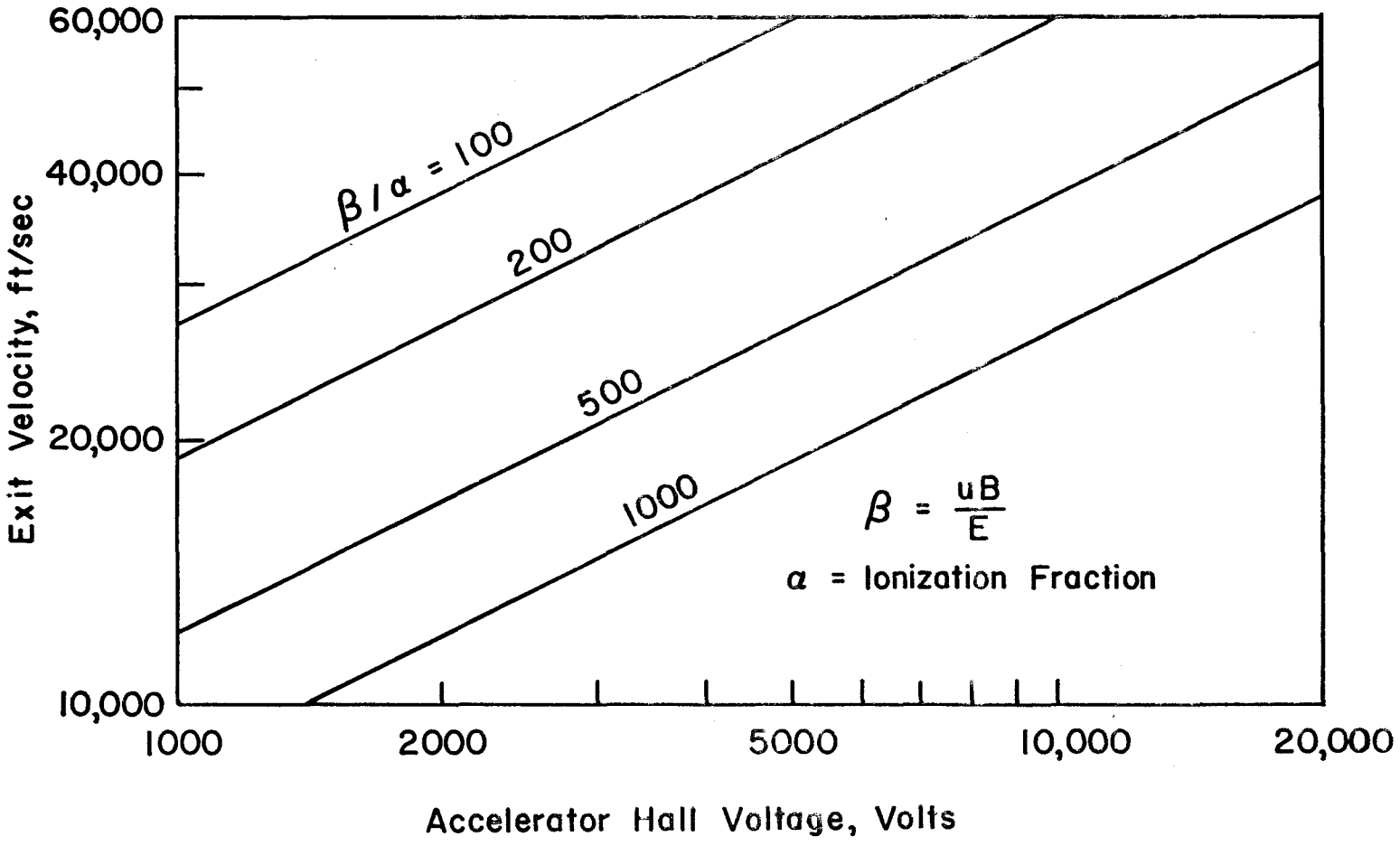

Fig. 6 Faraday Accelerator Hall Voltage, for Hall Currents Neutralized

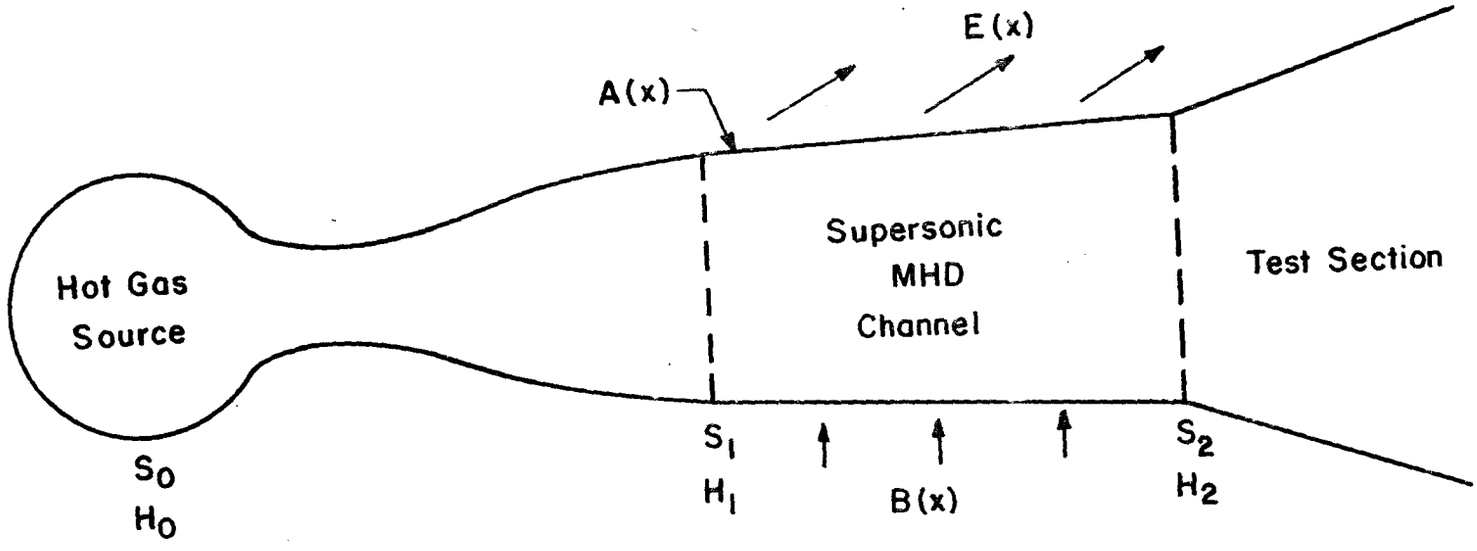

Fig. 7 Schematic of MHD Accelerator Configuration

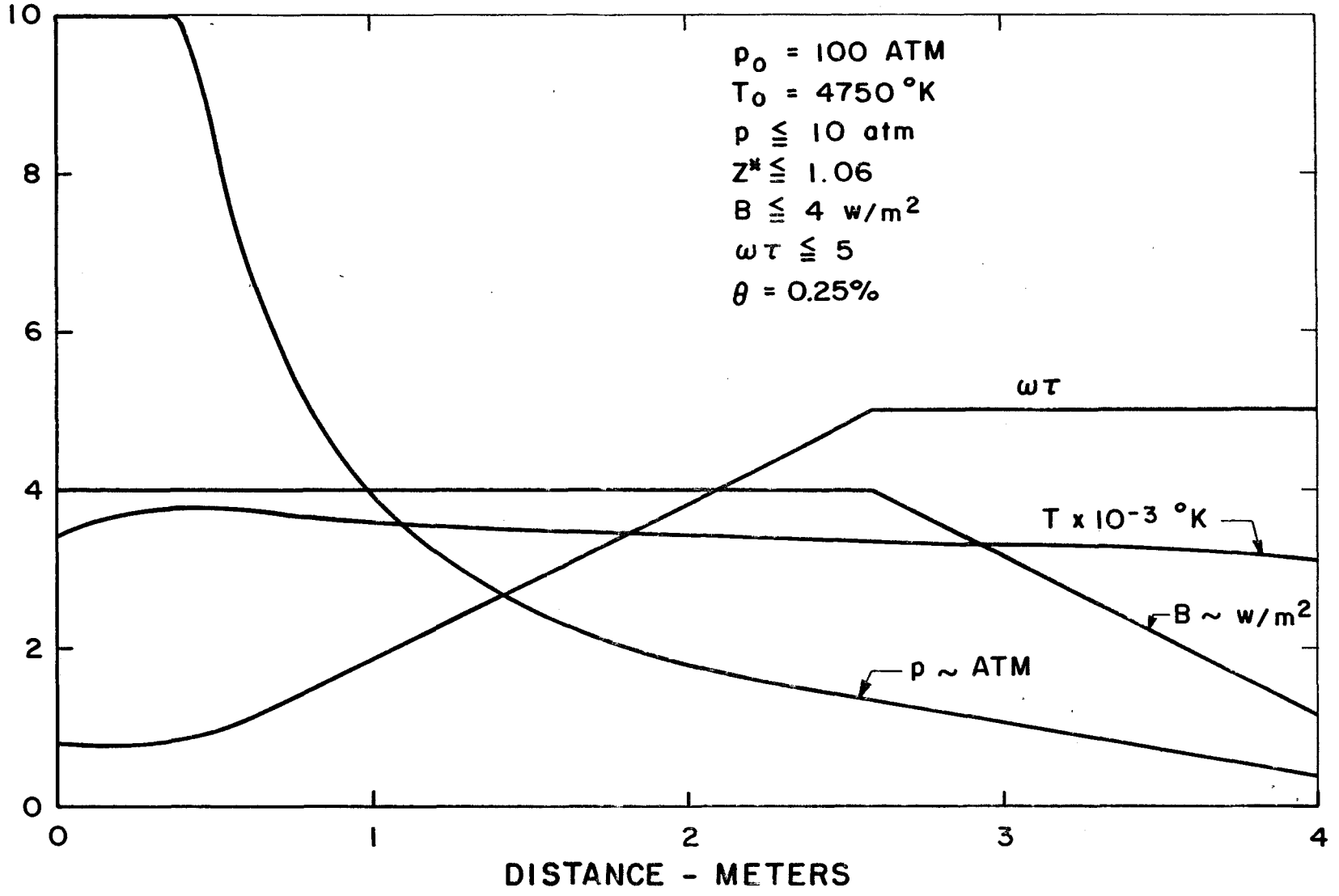

a. Pressure, Temperature, Magnetic Field, and Hall Coefficient

Fig. 8 Optimum Accelerator for 100-atm Arc-Heater

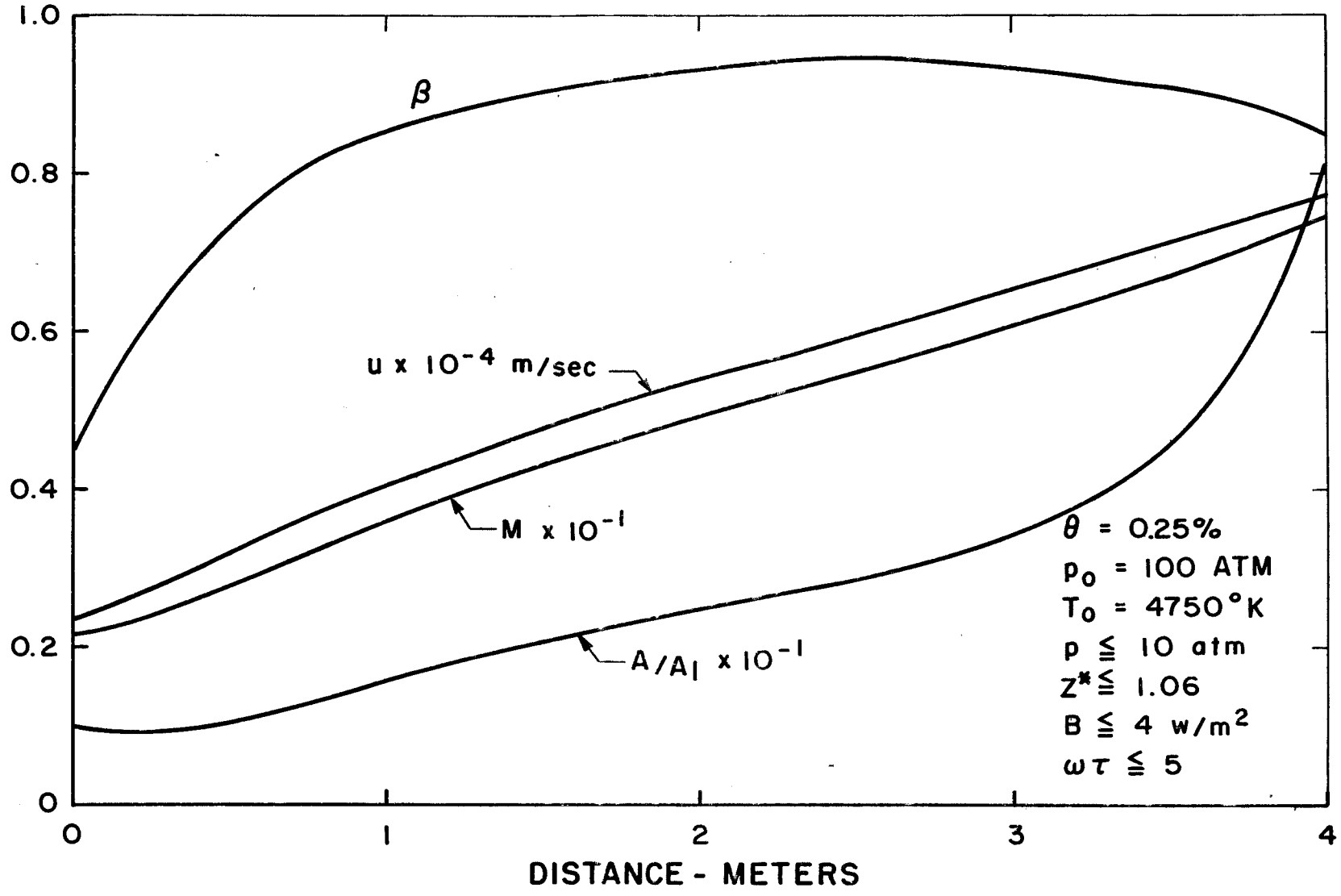

b. Area, Mach Number, Velocity, and β

Fig. 8 Concluded

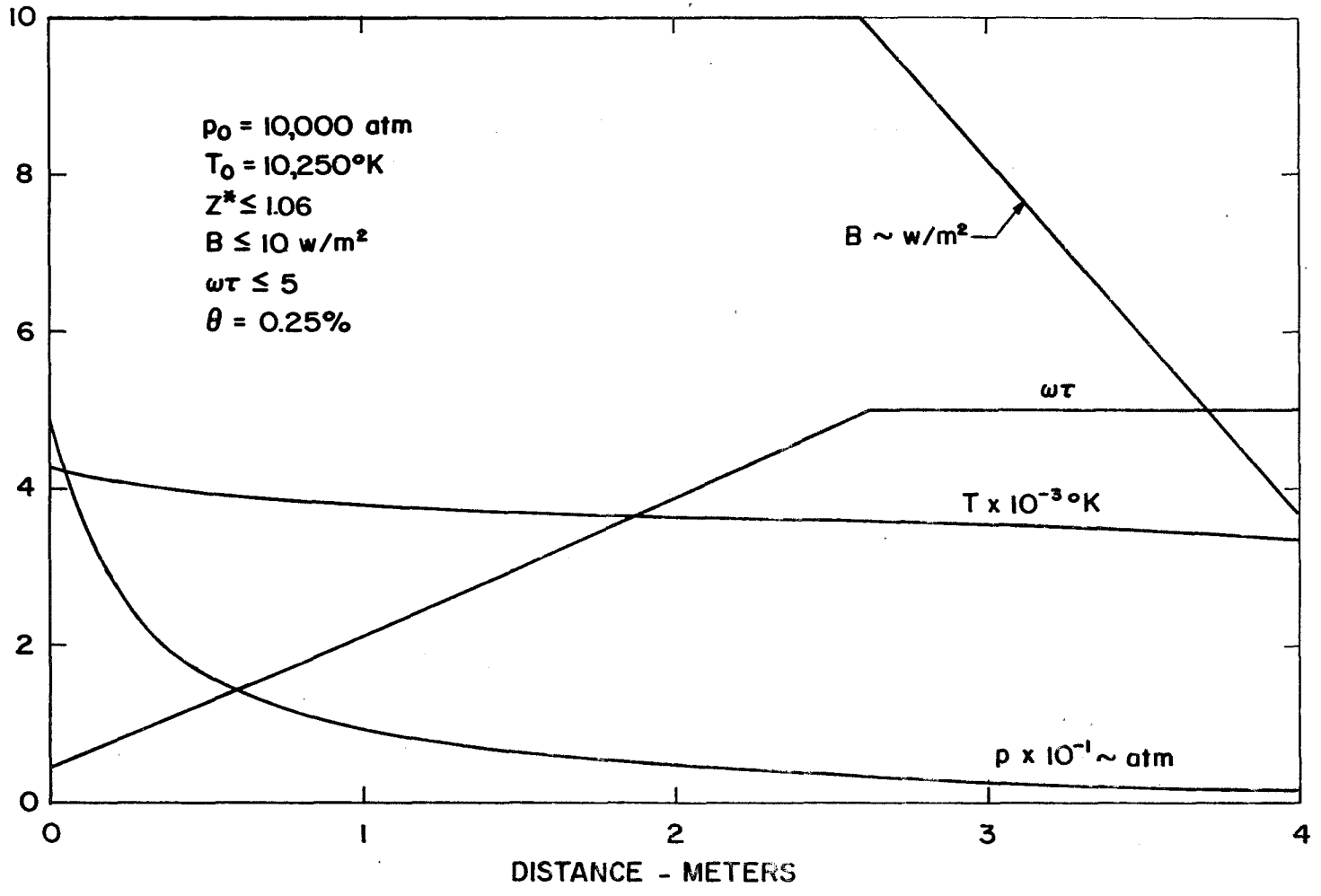

a. Pressure, Temperature, Magnetic Field, and Hall Coefficient

Fig. 9 Optimum Accelerator for Non-Reflected Shock Tunnel

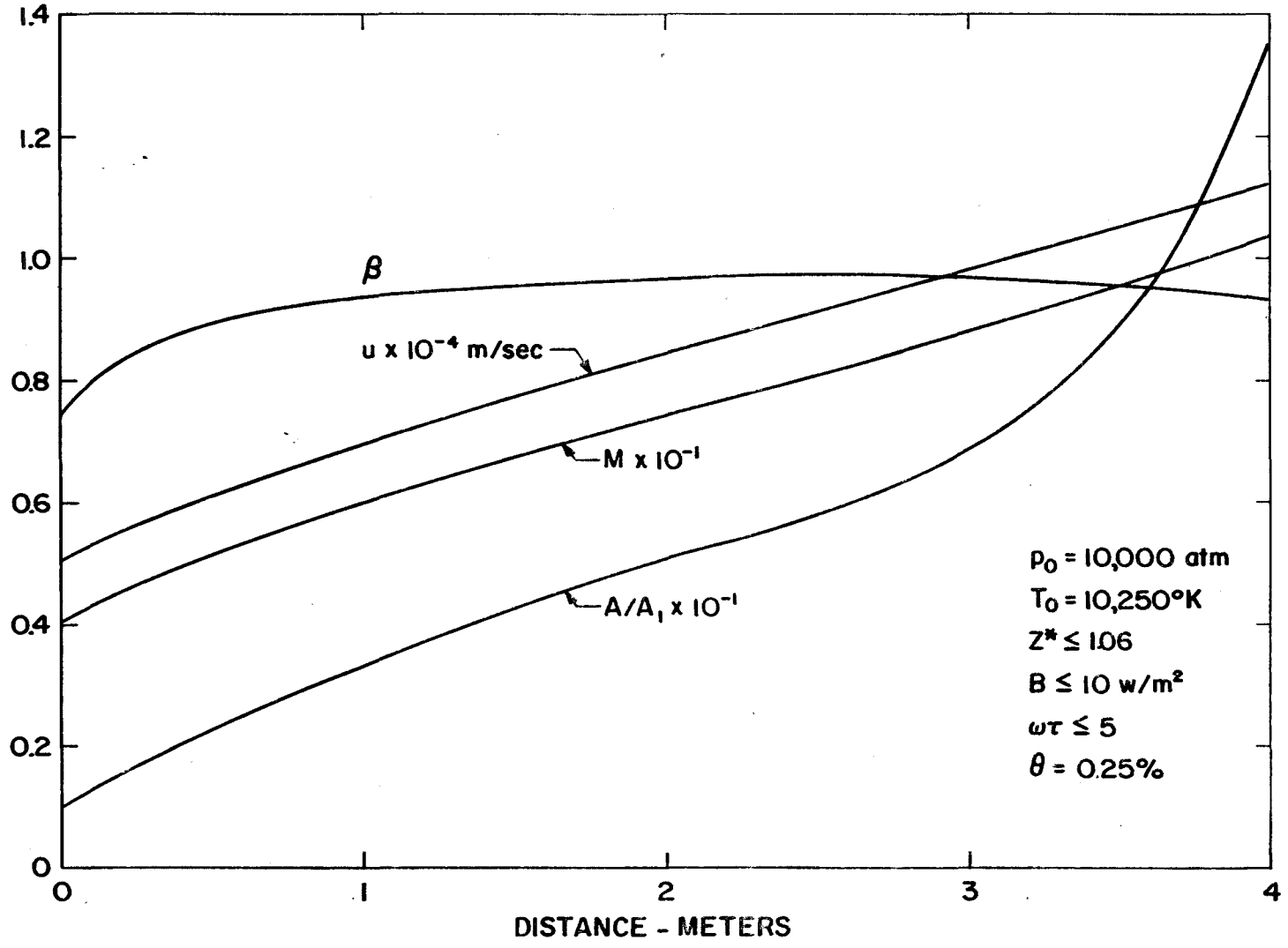

b. Area, Mach Number, Velocity, and β

Fig. 9 Concluded

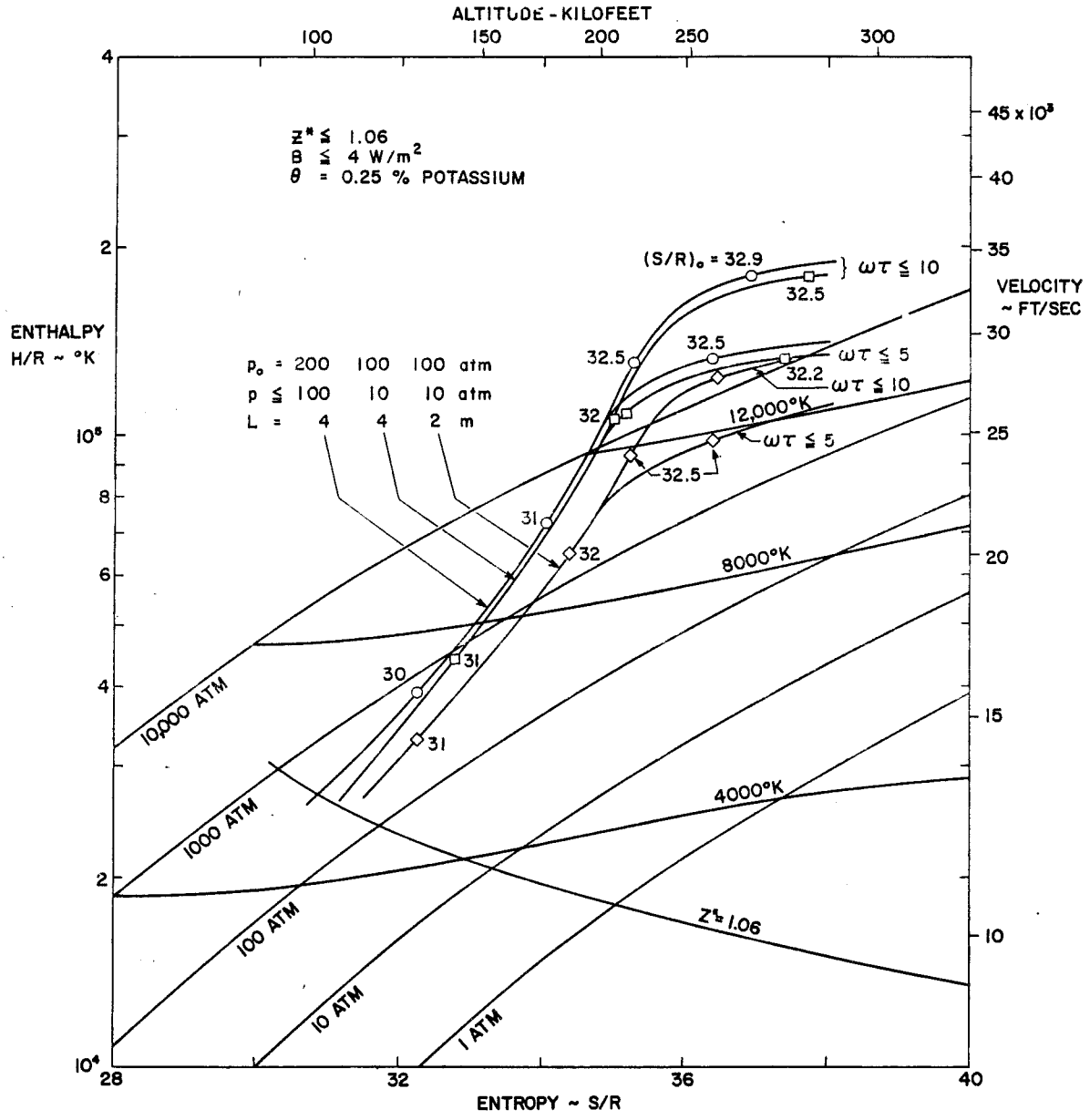

Fig. 10 Effect of Length and Reservoir Pressure on Faraday Accelerator Performance

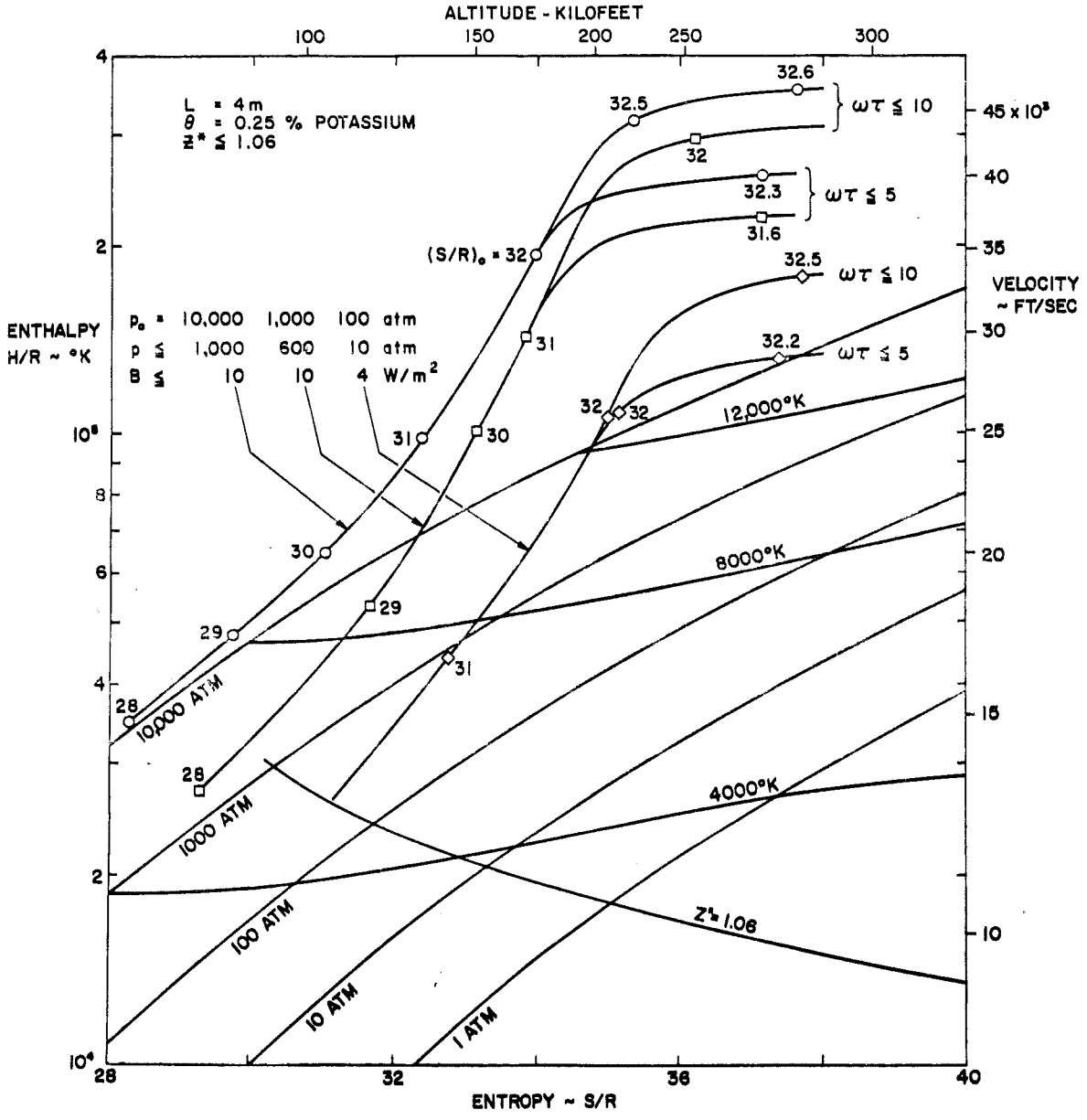

Fig. 11 Faraday Accelerator Limiting Performance